ABSTRACT

Docking Studies and Synthesis of a Gracilin A Derivative with Increased Predicted Affinity to Cyclophilin D

Zakariya Yazdani

Director: Daniel Romo, Ph.D, FRSC

Alzheimer's Disease (AD) is responsible for the progressive brain degradation of 3 million U.S. citizens annually and is the sixth leading cause of death in America. This disease has no current cure. The goal of this project is to synthesize a novel neuroprotective derivative of gracilin A. Gracilin A is a unique metabolite derived from the marine sponge *Spongionella gracilis* and member of the *spongiane* diterpenoid family. The new molecule will act as a potent inhibitor of pathways responsible for oxidative damage to neurons directly precursing the onset of AD.

Recently, derivatives of gracilin A were synthesized, analyzed, and determined to be potent neuroprotectors and immunosuppressants. These derivatives exhibit such effects by binding to cyclophilin D (CypD) thereby blocking opening of the mitochondrial permeability transition pore (mPTP). Docking experiments were performed to predict derivatives of gracilin A which would exhibit selectivity in binding to a CypD which blocks the mPTP and enhances neuroprotection over binding to Cyclophilin A (CypA). The compound proposed for total synthesis is based on a pre-existing mono-acetoxy furanose derivative of gracilin, compound 29a. The new molecule is characterized by the presence of a diol and absence of a gem dimethyl group.

APPROVED BY DIRECTOR OF HONORS THESIS:

_____

Dr. Romo, Department of Chemistry and Biochemistry

APPROVED BY THE HONORS PROGRAM:

_____

Dr. Andrew Wisely, Interim Director

DATE: _____

DOCKING STUDIES AND SYNTHESIS OF A GRACILIN A DERIVATIVE WITH INCREASED PREDICTED AFFINITY TO CYCLOPHILIN D

A Thesis Submitted to the Faculty of

Baylor University

In Partial Fulfillment of the Requirements for the

Honors Program

By

Zakariya Yazdani

Waco, Texas

April 2021

TABLE OF CONTENTS

LIST OF FIGURES

LIST OF SCHEMES

ACKNOWLEDGMENTS

I would like to extend my gratitude to Dr. Romo, my thesis mentor, who allowed me into his Minipharma group and family as an honorary adopted son. I would also like to thank Dr. Hull and Dr. Xue for aiding me in the lab and answering all the reaction questions I had. All my accomplishments in the lab were made possible through these three outstanding mentors. I cannot repay them for the time they have each spent in enriching my undergraduate career.

CHAPTER ONE:

Introduction

The debilitating effects of Alzheimer's disease has led to extensive research into its pathophysiology.. The two hallmarks of this dementia are deposits of extracellular β-amyloid (Aβ) in senile plaques and the development of neurofibrillary tangles. This formation and deposition ultimately interrupts synapses and leads to a gross decrease in neurons.[1] Aβ plaques are formed via the improper cleavage of the amyloid precursor protein. This precursor is believed to play a role in cell health and proliferation, but its specific function is unknown.[2] The resulting Aβ monomers aggregate to form oligomers which join to form amyloid fibrils, ultimately leading to a development of plaques.[3] Under non-pathologic conditions, amyloid precursor protein is cleaved by α-secretase and γ-secretase, which creates soluble protein fragments.[4] However, if the precursor protein is cleaved by γ and β-secretases, the resulting fragment is insoluble and may accumulate as Aβ plaques for up to 10 years before AD symptoms become observable enough to elicit a diagnosis.[5]

The second characteristic pathology of AD, neurofibrillary tangles, occurs when the tau protein is hyperphosphorylated. Tau protein is associated with the stabilization of microtubules, and its phosphorylation is a critical step in removing tau from microtubules to allow for transport.[6] Hyperphosphorylation of tau results in microtubule structure failure and disruption of several cellular processes dependent on their proper function.

The hyperphosphorylated tau accumulates to form neurofibrillary tangles.[7] This aggregation, along with the impairment in cellular morphology, inhibits cellular functioning and leads to apoptosis.[8]

The large-scale manifestation of Aβ and neurofibrillary tangle deposition is atrophy in specific areas of the brain, typically beginning with the mesial temporal lobe.[1] Many theories have been proposed outlining the mechanism by which AD progresses, but its intricacies are still debated by researchers. One popular belief is that inflammation of the brain should be included as the third pathologic hallmark of AD. Researchers have found that the equilibrium between pro-inflammatory and anti-inflammatory signaling is disrupted in AD patients, and chronic inflammation of the brain occurs due to the continual release of cytokines by activated microglia cells.[5]

Due to AD's similarity to its sister dementias, diagnosis of AD is not definitive until a patient's brain tissue is evaluated histologically. However, modern medicine can differentiate AD from other dementias with 85% accuracy via a simple neurologic examination and patient history.[1] The criteria for diagnosing a patient with AD include: a clinically documented procurement of dementia, deficiencies in greater than 2 areas of cognition, slow onset and progressive decline of memory and mental functioning, no interruption in consciousness, development after the age of 40, and ruling out of brain disorders such as strokes or tumors which may cause similar impairments in cognitive function and memory.[1] New diagnostic guidelines include testing for low levels of cerebrospinal fluid beta-amyloid and Aβ deposits in the brain detected by positron emission tomography.[9]

The prognosis of AD is discouraging. Although the rate of disease progression is patient-dependent, cognitive deterioration is unavoidable. After an individual is diagnosed with AD they typically survive for an average of 7 years, but they usually lose the ability to walk in 6 months.[1]

Treatment of AD is similar to guidelines followed for treatment of all other forms of dementia. The living area of an AD patient should be designed to emphasize orientation, with placement of clocks and calendars in accessible locations. The atmosphere should be bright and familiar, with safety measures such as monitors implemented. Caregivers should remain in contact with social workers and nurses to help ease stress involved with assisting an AD patient, and to ensure proper care is being provided. Cholinesterase inhibitors such as rivastigmine, donepezil, and galantamine are the primary medications given to AD patients to enhance cerebral function and recall.[1]

As previously mentioned, Aβ peptide plaque deposits are a hallmark of AD.[10] Aβ deposits form when Amyloid Precursor Proteins present in cell membranes are cut by β and γ secretase, and consequently misfolded.[11] These misfolded proteins can form oligomers which aggregate and disrupt the synapses between neurons or may enter the cell and interact with metal ions to form reactive oxygen species which consequently induce oxidative stress ultimately leading to apoptotic cell death[11] (Figure 1).

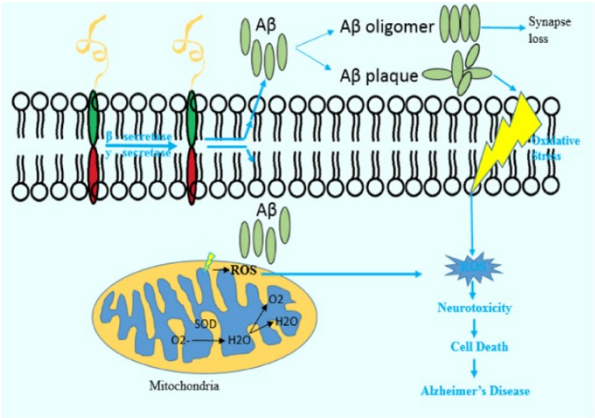

Figure 1. *Formation of Aβ deposits from Amyloid Precursor Protein*[2]

Aβ deposits which have re-entered the mitochondrial matrix may also complex with CypD and trigger the opening of the Mitochondrial Permeability Transition Pore (mPTP) via translocation of CypD to the inner mitochondrial membrane.[10] When the mPTP is opened via CypD, the cell becomes unable to retain its Ca^{+2} concentration and subsequently undergoes apoptosis.[12] Inhibition of CypD has shown to increase Ca^{+2} in the mitochondria and suppress oxidative-stress induced cell death.[12]

CHAPTER TWO:

Computational Chemistry: Docking Studies with *Molecular Operating Environment* (MOE)

A particularly interesting derivative of gracilin A is compound **29a** previously described as a promising lead (Figure 2). This derivative was synthesized and assayed with IC_{50} values indicating that this derivative has a higher selectivity to CypD over CypA relative to its GraA (Figure 3).

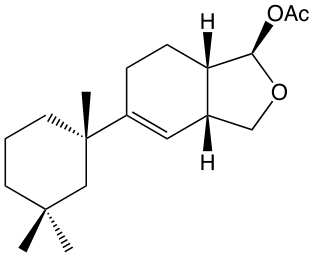

	Binding affinity (kcal/mol)	PPIase IC50
CypD	-83	0.018 μM
CypA	-76	0.32 μM
Selectivity	7	

Figure 2. *Compound 29a docking scores compared to IC50 data*

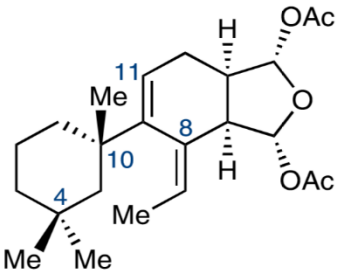

Gracilin A (**1**)

Viability(%):	94.6 ± 4.6% (0.1)
TMRM (%):	78.5 ± 1.9% (1.0)
ROS (%):	96.9 ± 9.2% (0.1)
GSH (%):	>10.0 μM
mPTP blockage:	103.6 ± 15.2% (0.1)
CypD (IC_{50}, μM):	0.26 μM (CI:0.12–0.6)
CypA (IC_{50}, μM):	0.27 μM (CI: 0.13–0.51)

Figure 3. *Activity of gracilin A as a neuroprotective compound*[4]

Using a program called Molecular Operating Environment (MOE), we were able to virtually dock and modify derivatives of compound **29a** to CypA and CypD. MOE predicts how well molecules interact with binding sites and produce outputs in units of kcal/mol to score binding affinities. Using MOE, we were able to dock hundreds of derivatives of compound **29a** in search of a more selective compound (Figure 4). In general, an important caveat to keep in mind with modeling studies is that these studies can suggest what not to synthesize more than what to synthesize.

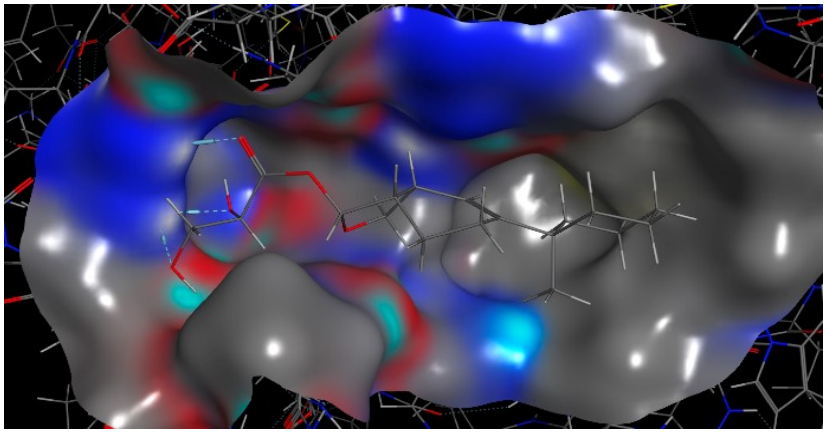

Figure 4. *Derivative of compound 29a docked into Cyclophilin D using the Molecular Operating environment*

Criteria we considered in selecting a derivative for synthesis included: binding affinity to CypD, selectivity to CypD over CypA, and feasibility of synthesis. The compound we selected contains a higher predicted binding affinity to CypD over CypA, greater selectivity, and predominately follows the same synthetic route to compound **29a**

(Figure 5). Changes to the original derivative **29a** include the removal of the gem-dimethyl group and the addition of a diol group to the polar portion of the compound.

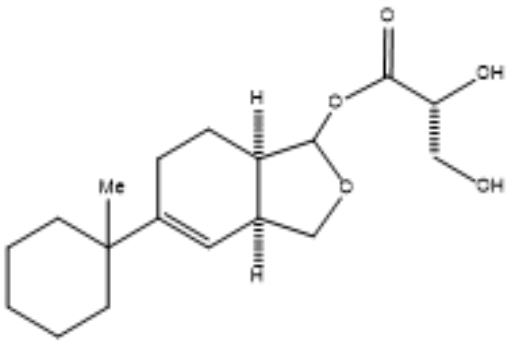

CypD (kcal/mol)	-98.4
CypA (kcal/mol)	-76.7
Selectivity	21.7

Figure 5. *Derivative of compound 29a chosen for total synthesis*

Stability Studies

The acetoxy region of GraA is susceptible to hydrolysis by the enzymes present in human plasma. To consider this compound as a potential pharmacological agent, we must first test its stability in physiological conditions. Therefore, we have run a stability study of an analogous derivative (Figure 6) of GraA in human plasma to determine the compound's half-life (Figure 7). This study was run in triplicate and the mearured half-life is ~2.9 hours. The same test was run in triplicate on derivatives **29a** (Figure 8) and **16**; a sulfonamide-containing compound (Figure 9). Our initial lead GraA derivative **29a**

(Figure 8), had the longest determined half-life (~15.7 h) by far of all three compounds tested.

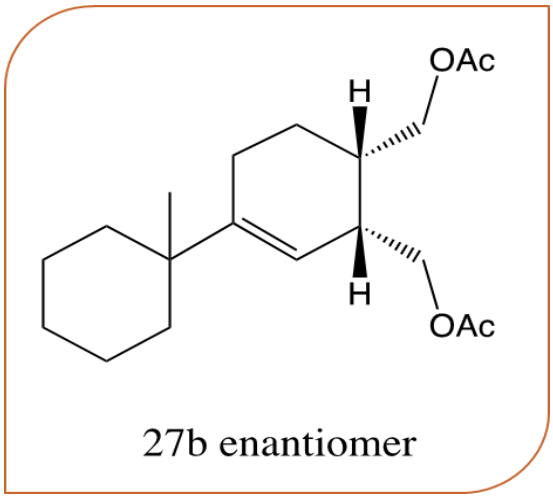

Figure 6. *Derivative of gracilin A, enantiomer of compound 27b*

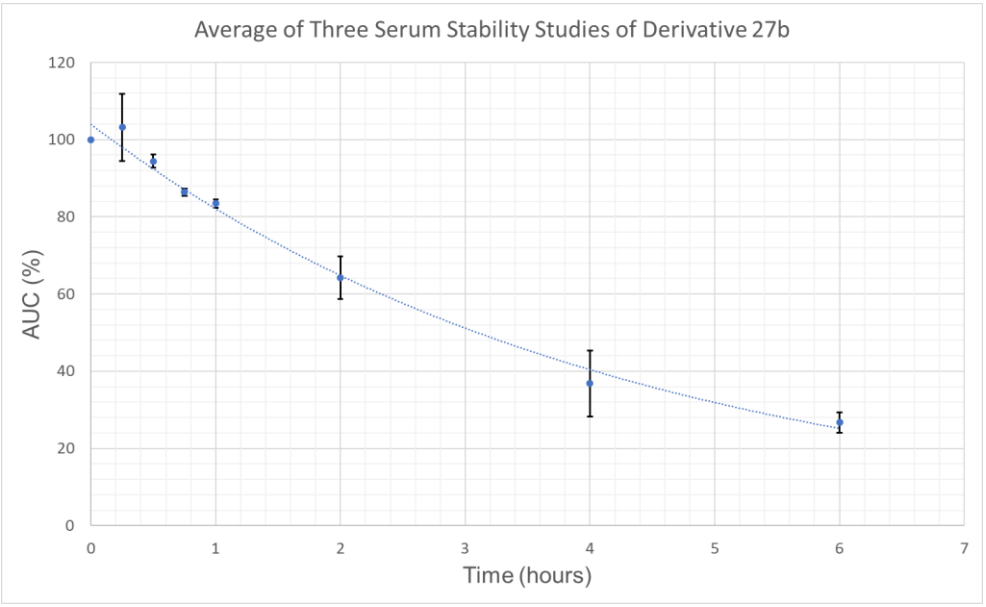

Figure 7. *Results of serum stability study of enantiomer of GraA derivative* ***27b***

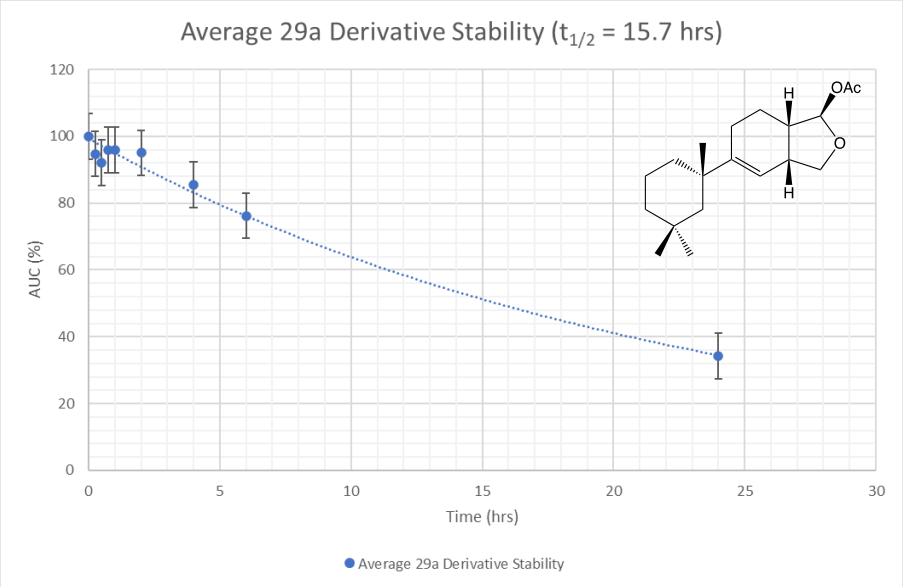

Figure 8. *Results from triplicate stability study of derivative **29a**.*

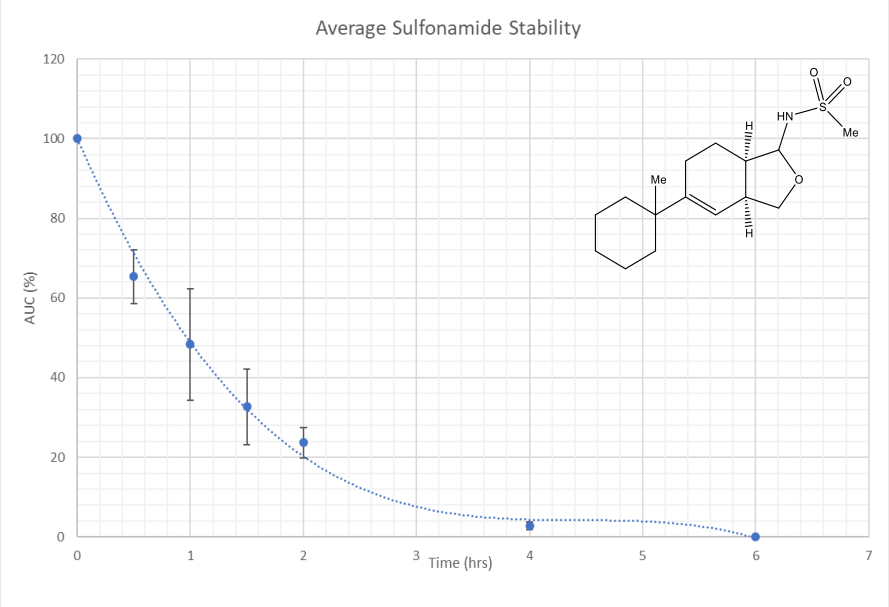

Figure 9. *Results from triplicate stability study of sulfonamide- containing derivative **16**.*

General Methods

Plasma Stability Studies General Procedure (Figures 11, 12, 13)

In a 1 dram vial, 400 to 900 μg of GraA derivative was dissolved in 90 μL of dimethyl sulfoxide (DMSO). This solution was added to 900 μL of human serum from Sigma Aldrich in a 1 dram vial and stirred at 37 °C. Several 100 μL aliqouts were taken at 7 time periods (usually 0 min, 30 min, 1 h, 2 h, 4 h, 6 h, and 24 h, depending on the stability of the specific derivative) and added to 400 μL acetonitrile (CH_3CN). This solution was then vortexed for 25 seconds and centrifuged at 12,000 rpm for 2 min. The supernatant was transferred to a 2 mL Agilent HPLC vial and 50 μL of sample was injected into an Agilent 1200 Series HPLC using a reversed-phase Gemini 3 μm NX-C18 Analytical 150 x 4.6 mm column and run using a typical gradient of 20% to 95% ACN/water for 15 minutes detecting at a wavelength of 210 nm (UV). The UV peaks were integrated and normalized as a percentage of the derivative at time zero. The half-life was calculated from the average of the data run in triplicate.

CHAPTER THREE:

Identification of Selective CypD over CypA Inhibitors

CypA is an immunophilin protein which plays an integral role in intracellular and extracellular inflammatory response.[13] CypA uses its peptidyl prolyl *cis-trans* isomerase activity to moderate the folding and trafficking of proteins in the cytosol of cells, but it also has the ability to be secreted to trigger endothelial inflammation. CypA has proven to a be critical component in many human diseases including cardiovascular diseases, cancer, viral infection, rheumatoid arthritis, periodontitis, sepsis, and asthma.[13] Therefore, its inhibition would doubtlessly yield complications in disease mediation. However, CypA overexpression is associated with poor reaction to inflammatory disease, metastasis of cancer, and aging.[13]

Cyclophilin A's role in Alzheimer Disease

One of the primary progenitors of neurodegenerative diseases like AD is oxidative stress.[14] CypA has been studied as a factor in diseases mediated by reactive oxygen species, and researchers have concluded that CypA is a necessary component in

the pathogenesis of diseases induced by oxidative stress.[15] CypA is reported to be directly involved in the development of AD. CypA drives an age-dependent breakdown of the blood-brain barrier by initiating the release of neurotoxic molecules from brain pericytes. This release, mediated by astrocyte-derived human ApoE4 results in neuron damage as synaptic dysfunction[16] (Figure 10).

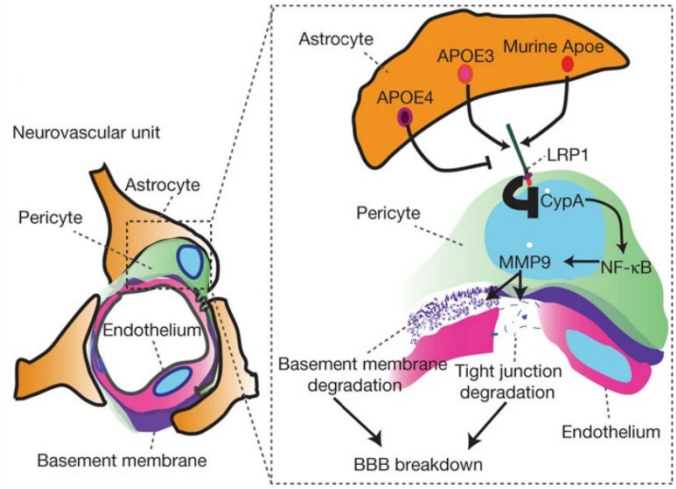

Figure 10. *Human ApoE3 and Murine Apoe silence a CypA pro-inflammatory pathway leading to neuronal dysfunction and neurodegeneration.*[16]

CypA also interacts with the transmembrane glycoprotein basigin to influence levels of Aβ peptide[17], one of the two aforementioned hallmarks of AD. The mechanism by which basigin regulates Aβ peptide levels is not fully understood.

A study conducted by Spisni *et al*.[18] concluded that CypA extracellular secretion is modulated by copper. An increase in extracellular copper levels causes a subsequent increase in radical oxygen species which triggers neurodegeneration via oxidative stress.

This same oxidative stress is correlated to CypA secretion as the body attempts to protect vulnerable neurons.[18]

Cyclophilin A as a drug target

Since CypA is a precursor to several human pathologies, attempts have been made to inhibit its activity. One of the most well-studied CypA inhibitors is the cyclic peptide cyclosporin A (CsA).[19] CsA is capable of binding CypA in the cytosol and when it is secreted. CsA silences CypA by inhibiting protein phosphatase calcineurin and the translocation of activated T-cell nuclear factor into the nucleus. The former process is involved in transcription of genes which induce inflammation.[20] CsA's inhibition of specific T cell responses is what made it a prime drug candidate for organ transplants.[21]

CypA is a complex protein with many functions. The current challenge faced by researchers is to find an inhibitor which selectively prevents damaging roles. And CsA does have some liabilities. Long-term CsA use causes kidney damage.[22] CsA's affinity to calcineurin is what causes problematic immunosuppression. Derivatives of CsA which lack this property have been synthesized in studies toward non-immunosuppressive drugs which may be used as an anti-viral agent for hepatitis C treatment.[23]

Our goal was to identify GraA derivatives with selectivity of CypD over CypA to avoid immunosuppressive effects while maintaining potential neuroprotective effects. Toward this goal, we used dockings studies with MOE to identify possible synthetic targets. This is because when GraA binds CypD it inhibits mitochondrial cell death

associated with AD, whereas the inhibition of CypA by GraA yields immunosuppressive effects.

CHAPTER FOUR:

Synthesis

***Scheme 1**. Synthetic route to GraA derivative **15**, starting with protection of glyceric acid (**1**) which is added to compound **13** via Shiina esterification.*

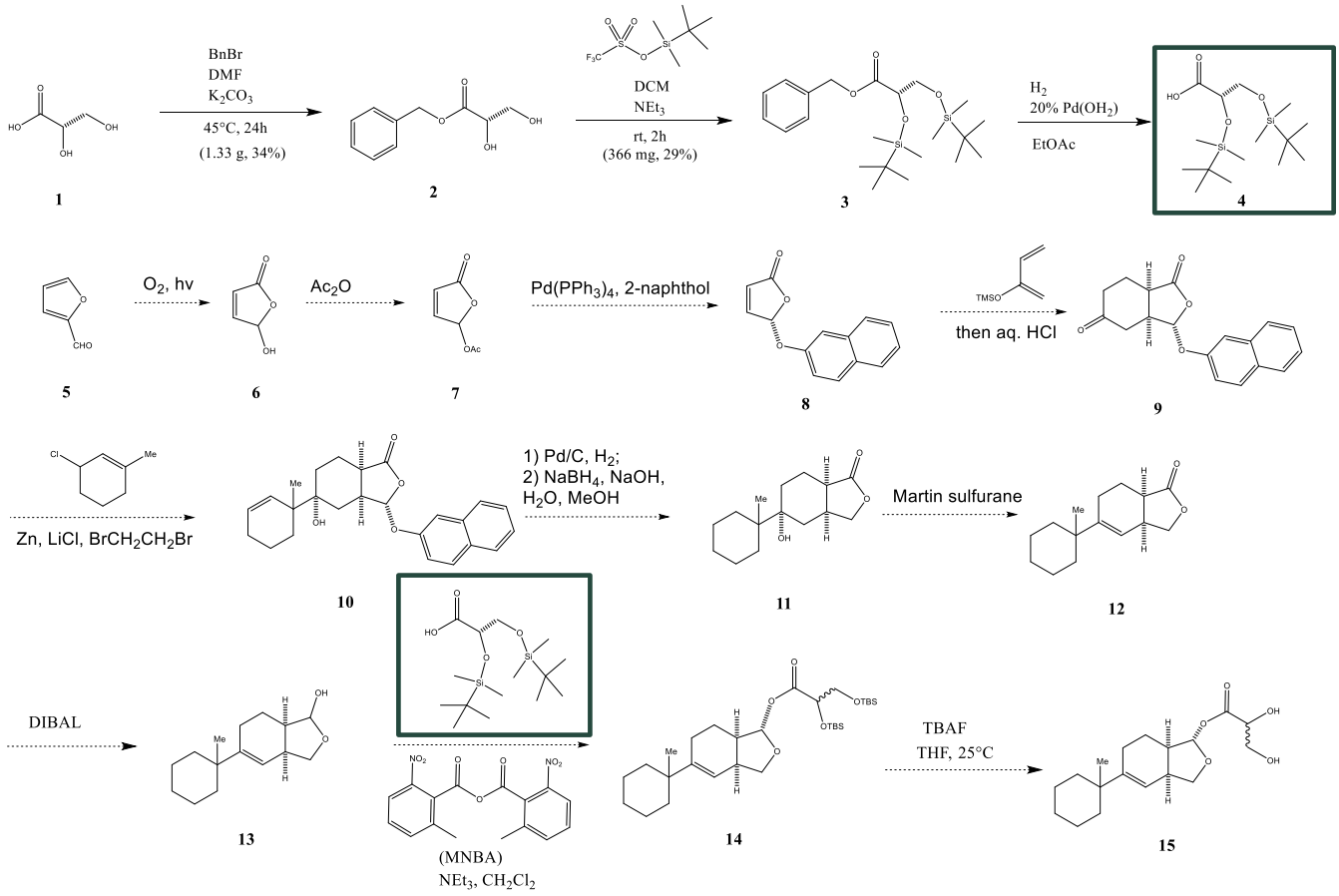

The first step of this synthesis is to protect the diol group of the glyceric acid (**1**) which will be used to esterify lactol **13** through Shiina esterification. In order to assure that the t-butyldimethylsilyl (TBS) groups attached to the primary and secondary hydroxyl groups, the carboxyl group was first benzylated (**2**). After sufficient material was obtained, protection of the diol was studied next. First, dichlorodiisopropyl silane was used to produce benzyl (*S*)-2,2-diisopropyl-1,3,2-dioxasilolane-4-carboxylate (**3a**), but the resulting ester was not stable after hydrogenation of the benzyl group. TBS was then used as it is more likely to remain attached to the diol under hydrogenation conditions. Alcohol protection was completed using TBSCl (**3b**), and then more successfully with TBS trifluoromethanesulfonate (triflate) to provide full protected ester **3**. Compound **3** is a novel derivative, so full characterization (HRMS, FTIR, ^{13}C NMR) was performed. Using TBS triflate lead to a much higher yield of diol protected product, minimizing mono-hydroxy protection, in shorter reaction times relative to the 2-day reaction with TBSCl. A small-scale hydrogenation of compound **3** was performed to yield the diol-protected carboxylic acid **4**. TLC and ^{1}H NMR provided evidence for a successful benzyl group removal leading to carboxylic acid **4**.

Scheme 2. *Protection of diol ester (**2**) using dichlorodiisopropylsilane.*

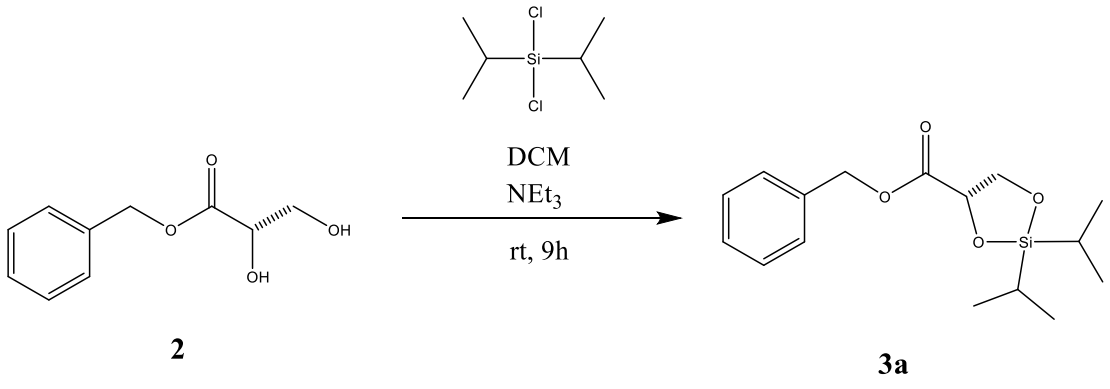

2 **3a**

Scheme 3. *Protection of diol ester (**2**) using TBSCl.*

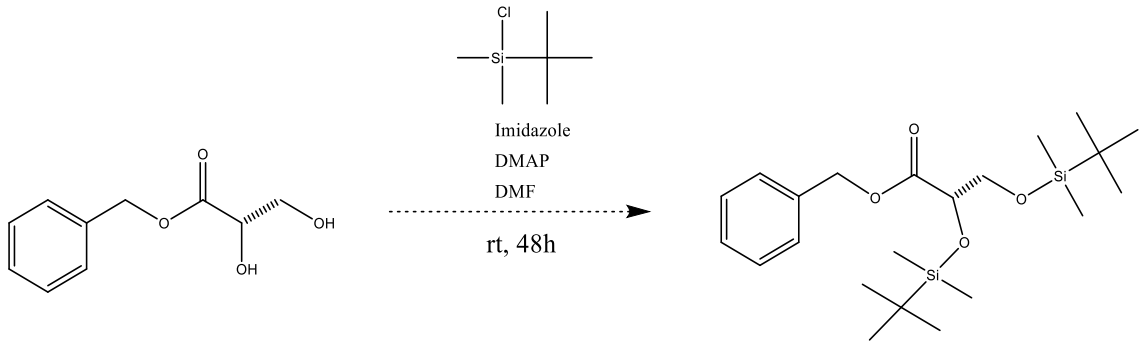

2 **3b**

Scheme 4. *Protection of diol ester (**2**) using TBS triflate.*

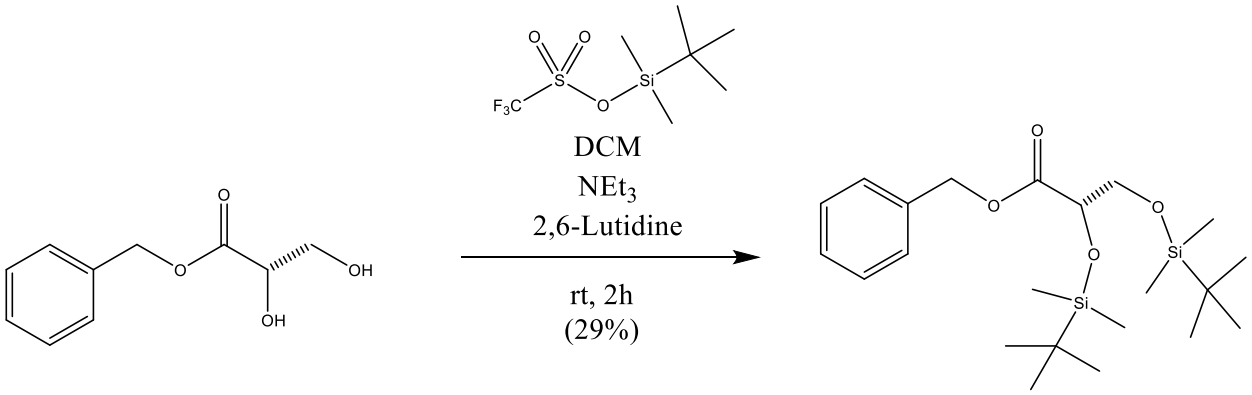

2 **3**

Scheme 5. *Removal of benzyl protecting group via hydrogenation*

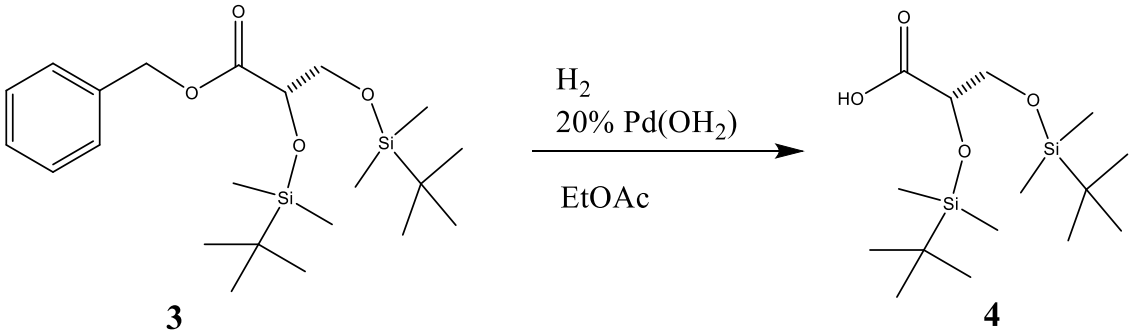

3 **4**

Future Plans

We recently repeated the first two steps of the synthetic route on large scale (2.5 g of the glyceric acid). A small-scale hydrogenation was conducted of benzyl ester **3** to determine the stability of silyl ethers after removal of the benzyl group. The remaining ester will be hydrogenated to enable esterification of the GraA skeleton following conversion of napthyl hydroxy lactone **10** to lactol **13** to esterify with the diol-protected carboxylic acid **4**. We will also perform additional serum stability studies of the targeted GraA derivative **15** and samples of this compound will be sent to collaborators for biological assay.

General Methods

Synthesis

Chemicals were purchased from Aldrich and used without purification. Experimental reactions were performed under anhydrous N_2 conditions and monitored via thin layer chromatography (TLC) on silica. Purification of products was carried out via flash column chromatography using silica. ^{1}H NMR characterization was performed on a Bruker Ascend spectrometer (400 MHz) and a Bruker Fourier spectrometer (300MHz). Chemical shifts (δ) are expressed in ppm and are referenced to deuterochloroform and deuterated methanol. Fourier Transform Infrared (FTIR) spectra were recorded as thin films on NaCl plates. High-resolution mass spectra were obtained through Baylor's Mass Spectrometry Center (BU-MSC). Abbreviations: h, hours; equiv, equivalents.

Synthetic Procedures:

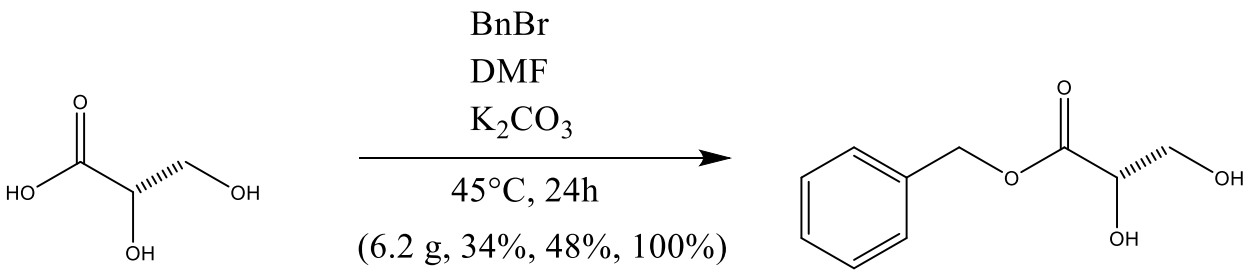

1 2

Formation of benzyl (*S*)-2,3-dihydroxypropanoate (2). 20% glyceric acid in water was freeze dried to obtain pure glyceric acid (yellow oil). To a dry flask under N_2 gas was added potassium carbonate (7.8 g, 56.43 mmol, 2.5 equiv) via funnel. Next, DMF (20 mL) and was added and spun at 600 revs per second. Glyceric acid (2.39 g, 22.6 mmol, 1 equiv) was freeze-dryed via lyophilizer and dissolved in DMF (10 mL) and the mixture was added to the solution via needle and septum. The solution was stirred for 24 hours at 45°C. Next, a glass-sintered funnel (C) was used to filter out potassium carbonate. Rotary evaporation and high vacuum were used on the reaction mixture to remove DMF. The crude material was purified by MPLC using a 120 mg large column and medium sized top column loader (MeOH/CH_2Cl_2: 0⟶20%) to yield 1.19 g product (48% yield). R_f = 0.5 (10% MeOH/CH_2Cl_2). ^{1}H NMR (400 MHz, MeOD) δ 7.48 – 7.25 (m, 5H), 5.33 – 5.12 (m, 2H), 4.27 (dd, *J* = 4.9, 3.9 Hz, 1H), 3.87 – 3.73 (m, 2H). See Figure 11 for 400 MHz ^{1}H NMR.

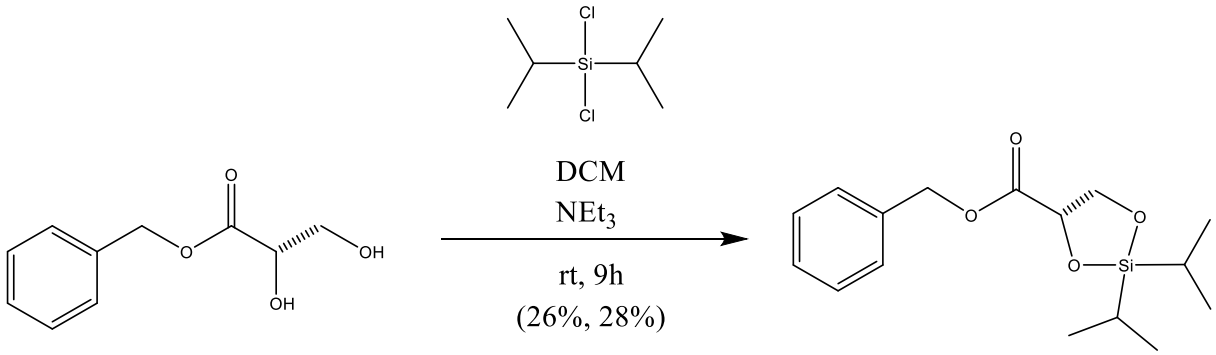

2 **3a**

Formation of benzyl (*S*)-2,2-diisopropyl-1,3,2-dioxasilolane-4-carboxylate (3a). To a 50 mL round-bottomed flask benzyl (*S*)-2,3-dihydroxypropanoate (210.5 mg, 1.073 mmol, 1 equiv) dissolved in 2 mL of dimethylformamide was added. Triethylamine (0.36 mL, 2.6 mmol, 2.4 equiv) was added to the solution. Finally, dichlorodiisopropylsilane (0.213 mL, 1.18 mmol, 1.1 equiv) was added to the flask. The solution was stirred at 500 rpm for 9 h at ambient (22 ºC) temperature. After 9 h, the reaction mixture was quenched with water (5 mL) and washed with ethyl acetate (3 X 20mL) in a separatory funnel. Sodium sulfate was added to the isolated organic layer, and the solution was poured through a paper filter into a flask. The solvent was evaporated from the crude product with a rotary evaporator. A crude NMR was taken before the product was purified via MPLC using a 12 g flash column and small loader (Ethyl Acetate/Hexanes: 0⟶50%) to yield 84.8 mg siloxane **3a** (26%) as an orange oil. R_f = 0.6 (Ethyl Acetate/Hexanes = 2:1). ^{1}H NMR (400 MHz, $CDCl_3$) δ 7.46 – 7.31 (m, 5H), 7.29 (s, 2H), 5.34 – 5.16 (m, 2H), 4.31 (dt, *J* = 6.7, 2.8 Hz, 1H), 4.13 (qd, *J* = 11.2, 2.8 Hz, 2H), 3.40 (d, *J* = 6.6 Hz, 1H), 2.59 (s, 1H), 1.56 (s, 5H), 1.09 – 0.94 (m, 14H), 0.94 – 0.73 (m, 2H). See Figure 2.A for 400 MHz ^{1}H NMR.

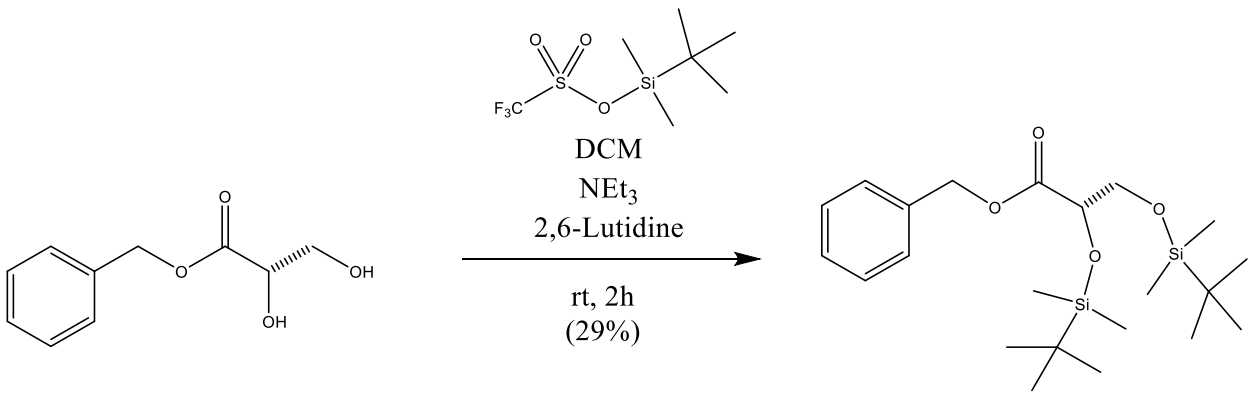

2 **3**

Formation of benzyl (*S*)-2,3-bis((tert-butyldimethylsilyl)oxy)propanoate (3).

To a flask (100 mL round bottom) was added benzyl (S)-2,3-dihydroxypropanoate (**2**) (579 mg, 2.95 mmol, 1 equiv) dissolved in dichloromethane (5 mL). 2,6 lutidine (1.2 mL, 10.3 mmol, 3.5 equiv) was added with a stir bar and the solution was put under N_2 gas. The flask was then placed in an ice bath for 5 minutes to cool to 0°C. *Tert*-butyldimethylsilyl trifluoromethanesulfonate (1.7 mL, 7.4 mmol, 2.5 eq) was then added dropwise. The solution was stirred and monitored via TLC for 2 hours. The reaction mixture was quenched with water (5 mL) and washed with ethyl acetate (2 X 20 mL) in a separatory funnel. Sodium sulfate was added to the isolated organic layer, and the solution was poured through a paper filter into a flask. The solvent was evaporated with a rotary evaporator and high vacuum. The crude material was purified by MPLC using a 24g flash column and 24g loading column (Ethyl Acetate/Hexanes: 0⟶30%) to yield 365.7 mg (29.2%) of bis-silyl ether **3**. R_f = 0.9 (Ethyl Acetate/Hexanes = 1:10). ^{1}H NMR (400 MHz, $CDCl_3$) δ 7.60 – 7.01 (m, 6H), 5.22 – 5.02 (m, 2H), 4.26 (dd, *J* = 6.0, 4.8 Hz, 1H), 3.91 – 3.63 (m, 2H), 0.82 (d, *J* = 4.6 Hz, 19H), 0.31 – -0.21 (m, 12H). See Figure 15 for 400 MHz ^{1}H NMR. ^{13}C NMR (400 MHz, $CDCl_3$) δ 128.49 (2), 128.35 (2), 128.24, 74.3, 66.9, 25.9, 18.3, see Figure 19 for ^{13}C NMR; IR (thin film): 2929, 2857, 1755

(carbonyl), 1462, 1361, 1252, 1125, 830, 776, 733 cm^{-1}, see Figure 17 for FTIR; HRMS (ESI+) m/z calcd for $C_{22}H_{40}NaO_4Si_2$ $[M+Na]^+$: 447.2357, found: 447,2356. See Figure 18 for HRMS (ESI+).

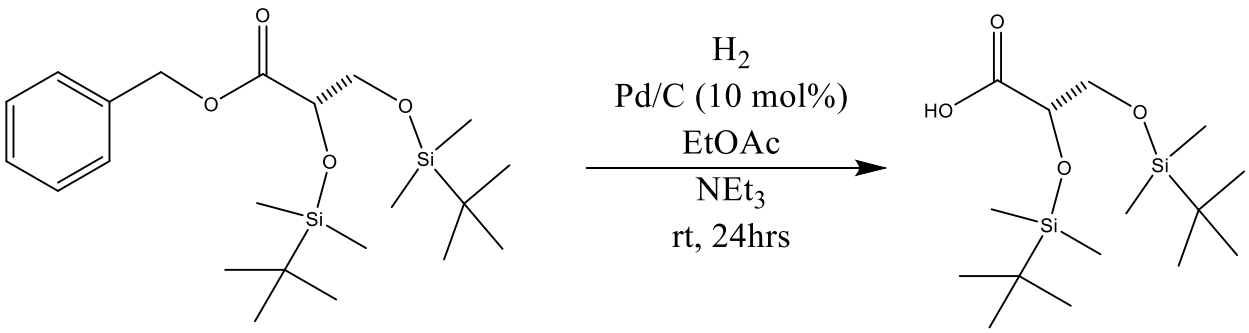

3 **4**

Formation of (*S*)-2,3-bis((tert-butyldimethylsilyl)oxy)propanoic acid (4).

To a 100 mL round bottom flask was added benzyl (S)-2,3-bis((tert-butyldimethylsilyl)oxy)propanoate (**3**) (352 mg, 0.829 mmol, 1 eq) dissolved in 10 mL of ethyl acetate. Palladium on carbon was added at 10 mol % (180 mg, 0.0829 mmol, 0.1 eq), along with triethyl amine (0.231 mL, 1.658 mmol, 2 eq) and a stir bar. The reaction mixture was placed under hydrogen gas and stirred at 290 rpm After 30 h, the reaction mixture was filtered via celite and a glass-sintered funnel and dryed with rotary evaporation and high vacuum. R_f = 0.3 ($MeOH/CH_2Cl_2$= 1:10). ^1H NMR (400 MHz, $CDCl_3$) δ 7.17 (s, 1H), 4.22 – 3.52 (m, 5H), 2.97 (q, *J* = 7.3 Hz, 6H), 1.25 – 1.10 (m, 9H), 0.95 – 0.63 (m, 18H), -0.05 (s, 11H). See Figure 16 for crude 400 MHz ^1H NMR stacked against its starting material.

Figure 11

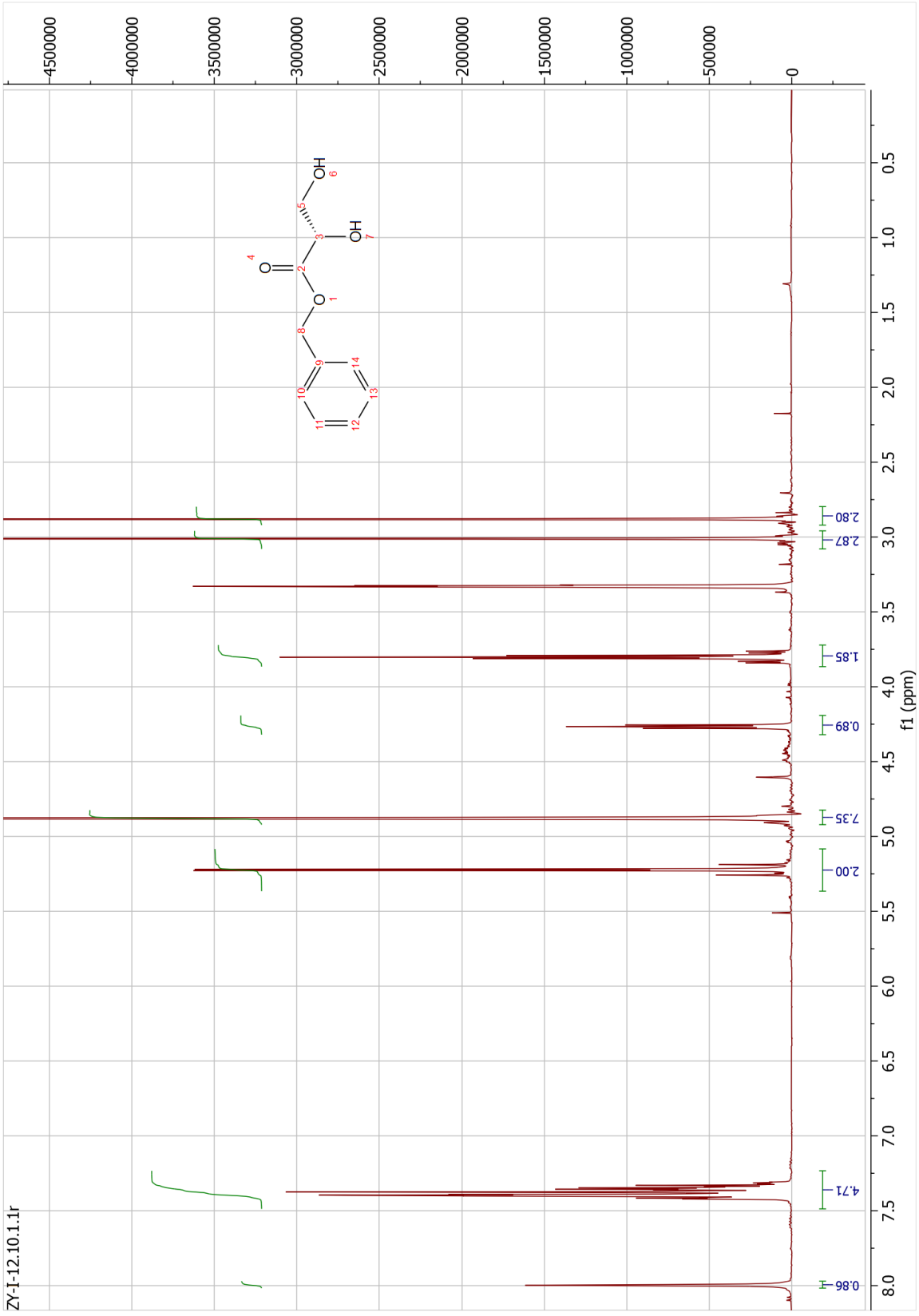

Figure 12

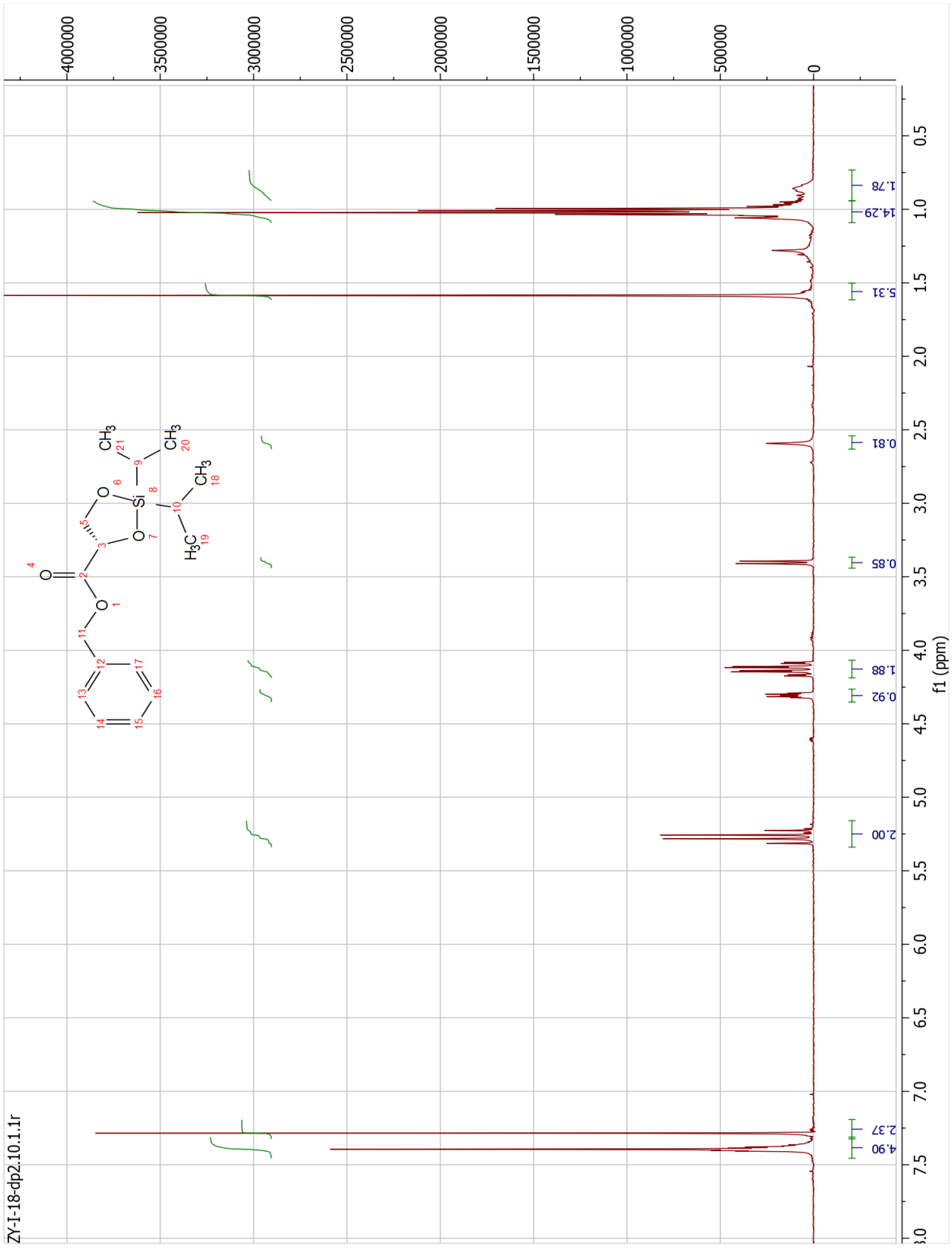

Figure 13

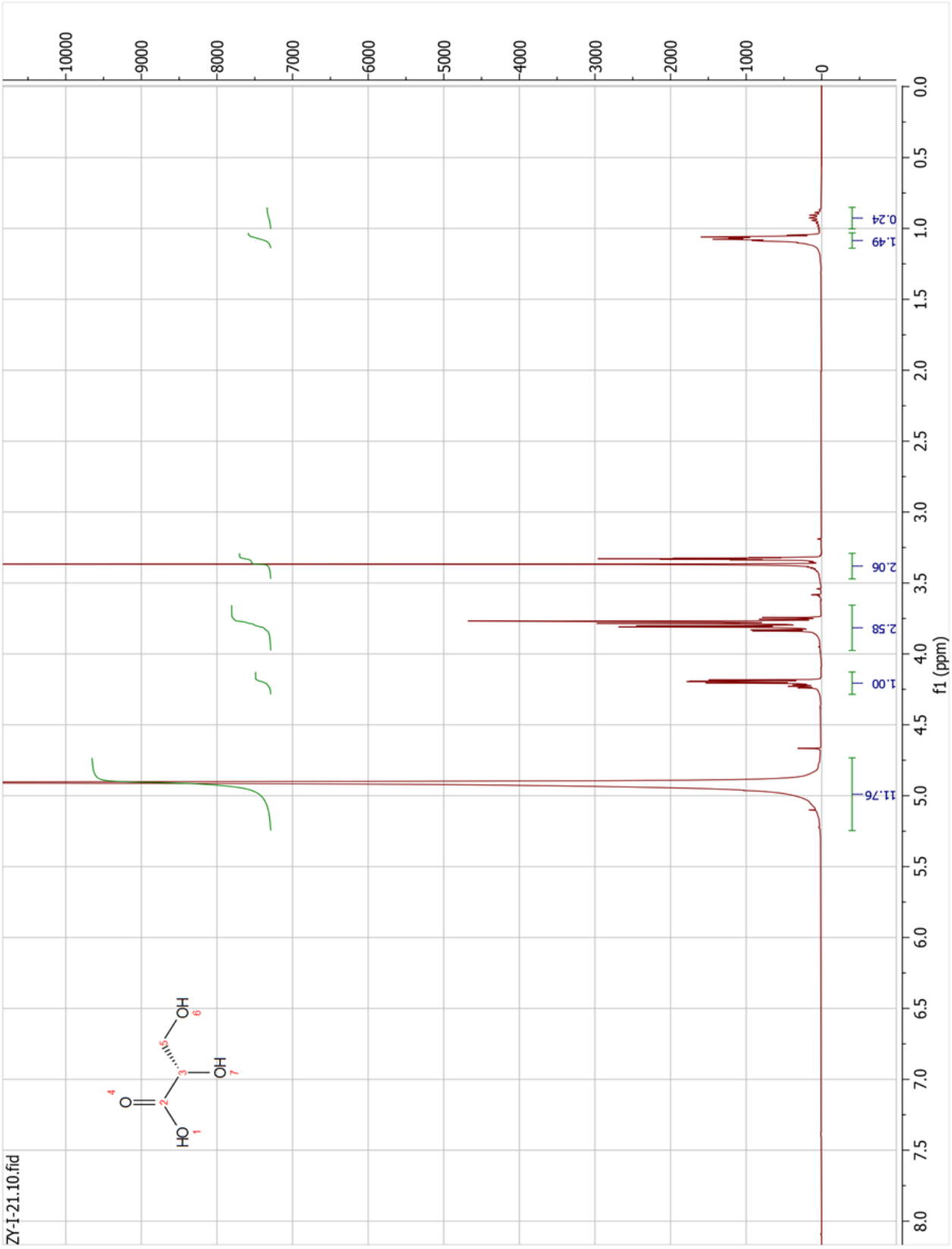

Figure 14

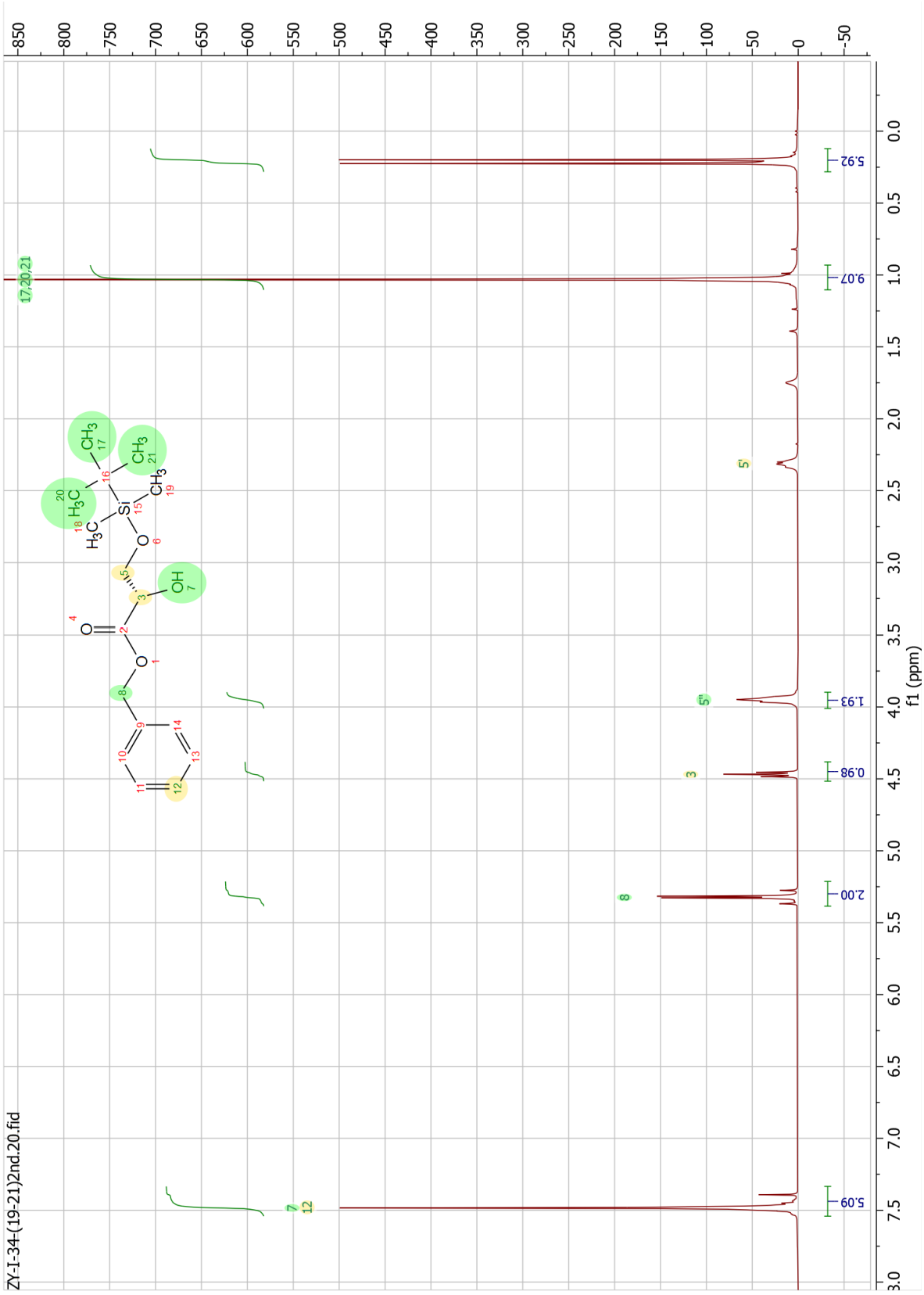
ZY-I-34-(19-21)2nd.20.fid
f1 (ppm)
17,20,21
12
8
3
5'
5''
5.92
9.07
1.93
0.98
2.00
5.09
OH
CH3
Si
O

Figure 15

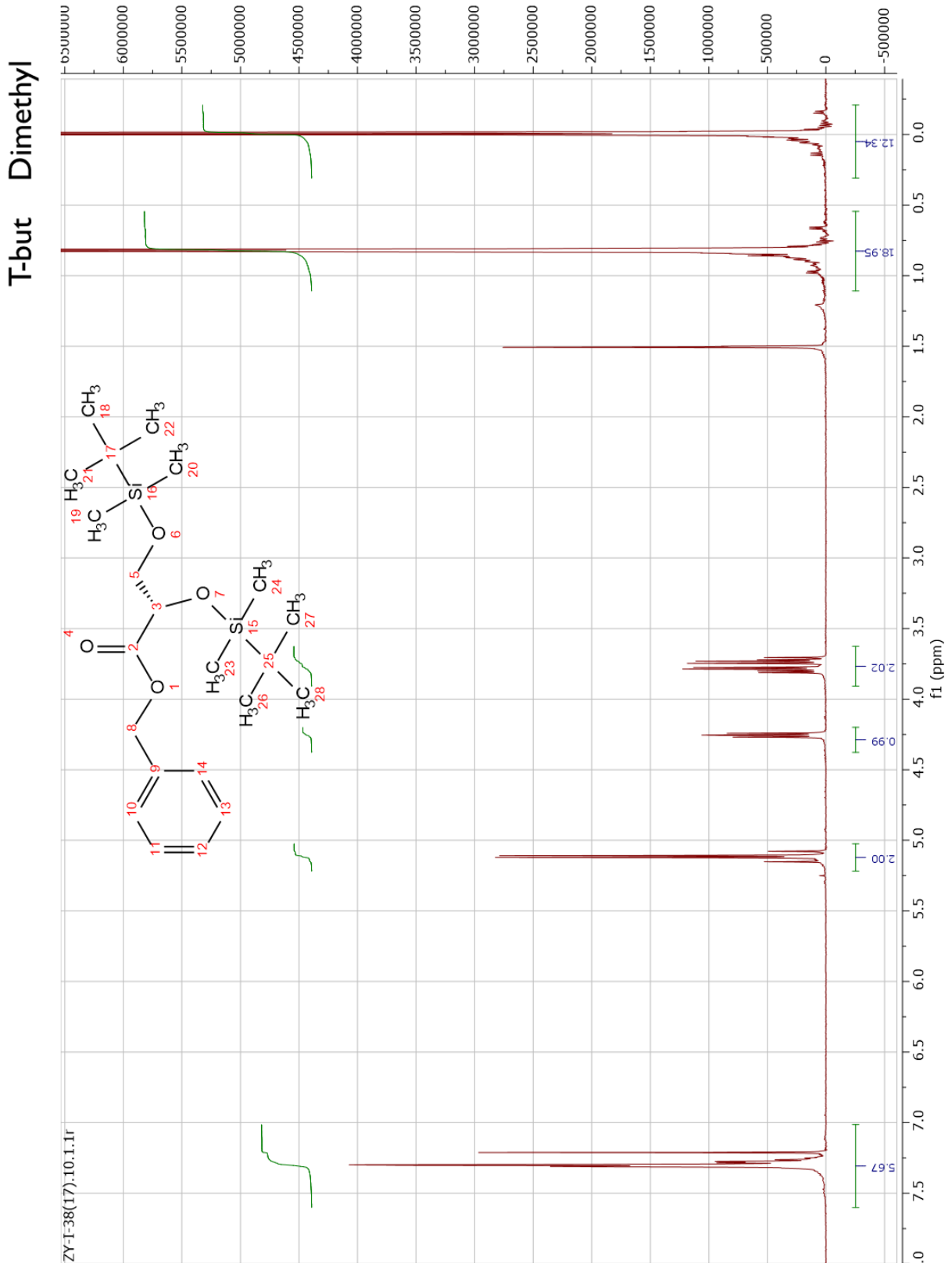

Figure 16

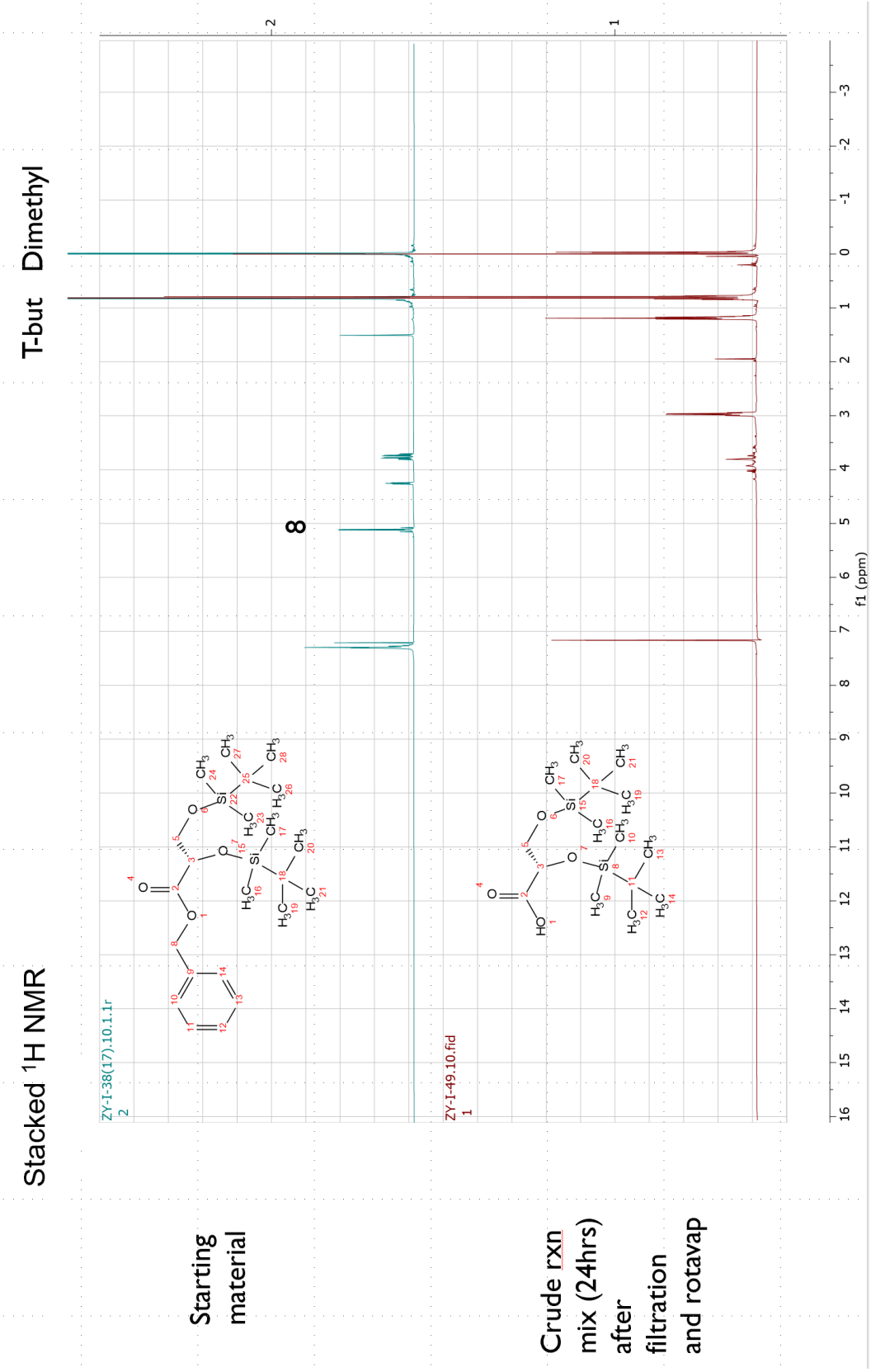
Stacked ¹H NMR
T-but
Dimethyl
8
ZY-I-38(17).10.1.1r
2
ZY-I-49.10.fid
1
Starting material
Crude rxn mix (24hrs) after filtration and rotavap
f1 (ppm)

Figure 17

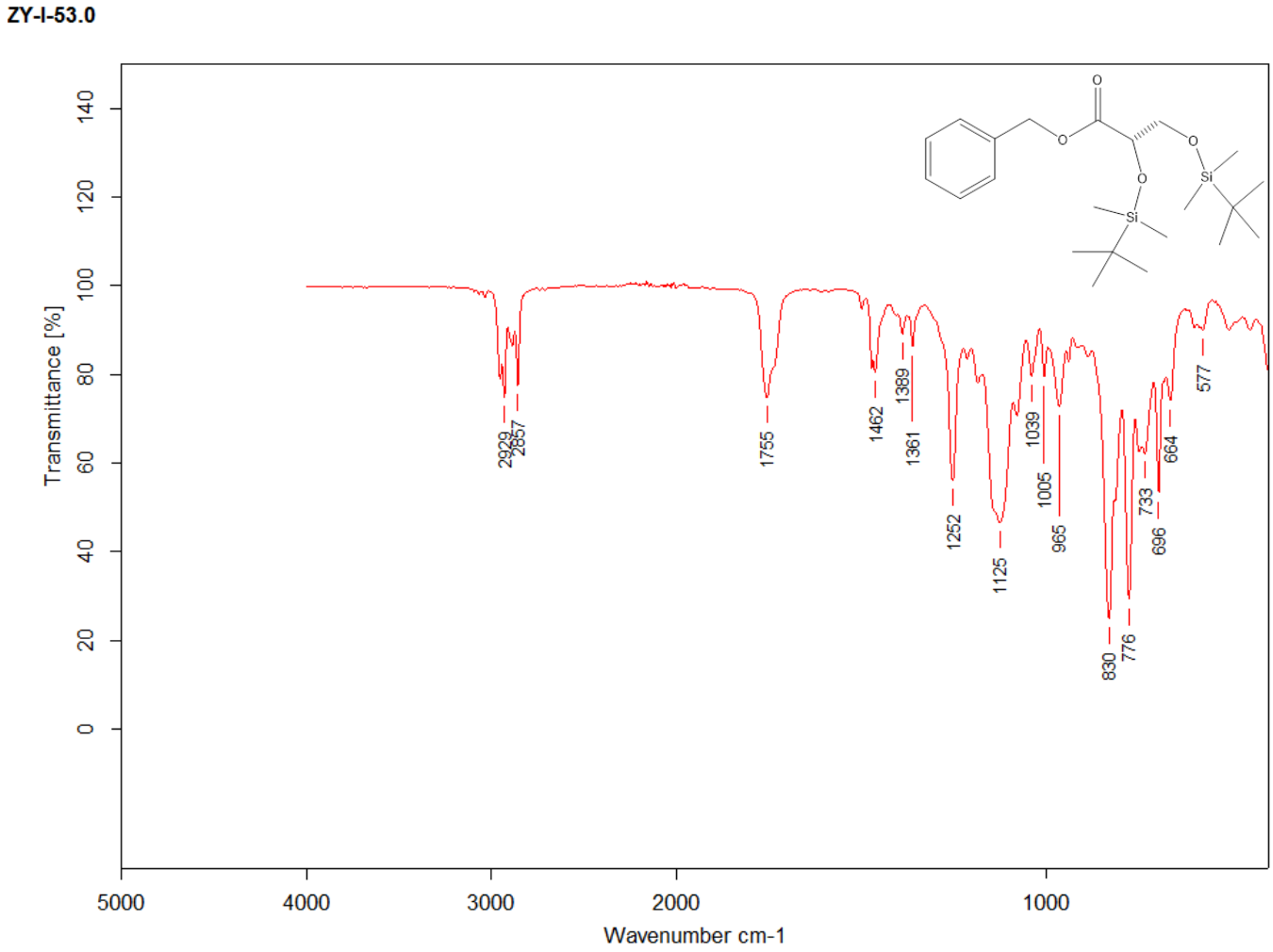
ZY-I-53.0
Transmittance [%]
0
20
40
60
80
100
120
140
5000
4000
3000
2000
1000
Wavenumber cm-1
2929
2857
1755
1462
1389
1361
1252
1125
1039
1005
965
830
776
733
696
664
577
O
O
O
Si
O
Si

Figure 18

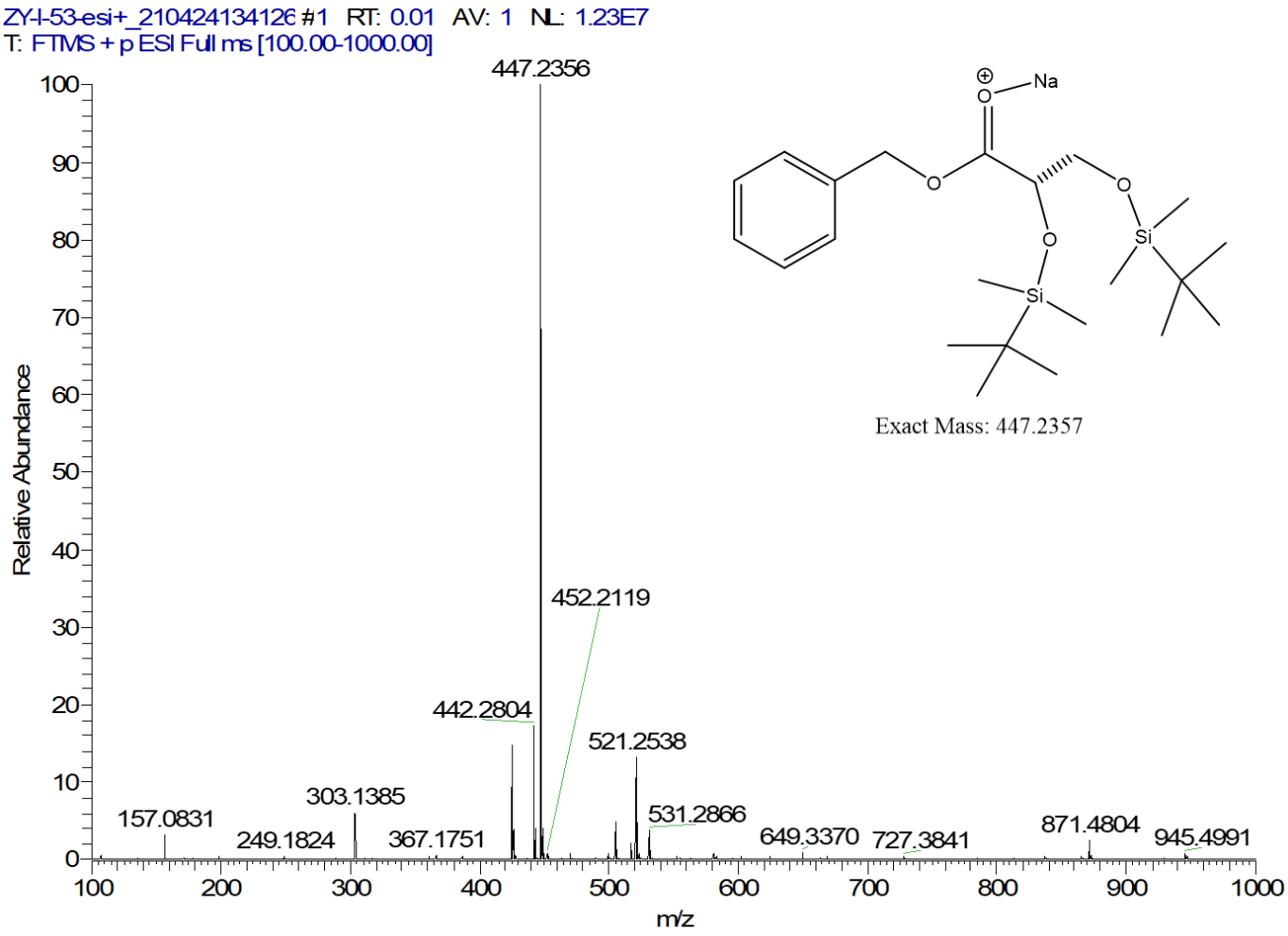
ZY-I-53-esi+_210424134126 #1 RT: 0.01 AV: 1 NL: 1.23E7
T: FTMS + p ESI Full ms [100.00-1000.00]
447.2356
452.2119
442.2804
521.2538
303.1385
157.0831
249.1824
367.1751
531.2866
649.3370
727.3841
871.4804
945.4991
Relative Abundance
m/z
Na
O
Si
Exact Mass: 447.2357

Figure 19

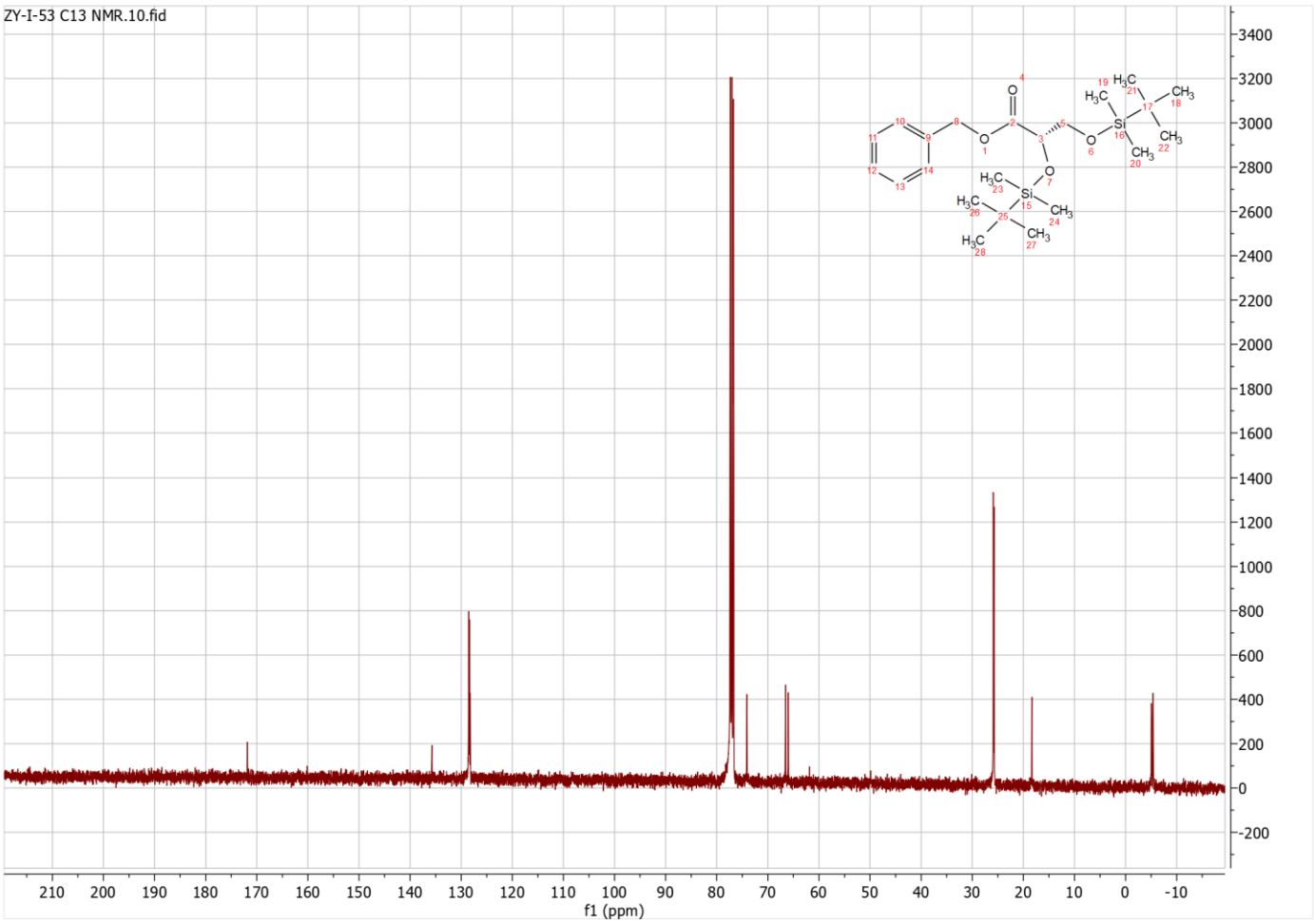

BIBLIOGRAPHY

1. Alzheimer Disease - Neurologic Disorders. Merck Manuals Professional Edition. Accessed April 3, 2021. https://www.merckmanuals.com/professional/neurologic-disorders/delirium-and-dementia/alzheimer-disease

2. O'Brien RJ, Wong PC. Amyloid Precursor Protein Processing and Alzheimer's Disease. *Annu Rev Neurosci*. 2011;34(1):185-204. doi:10.1146/annurev-neuro-061010-113613

3. Selkoe DJ. Normal and Abnormal Biology of the beta-Amyloid Precursor Protein. *Annu Rev Neurosci*. 1994;17(1):489-517. doi:10.1146/annurev.ne.17.030194.002421

4. Anderson JP, Chen Y, Kim KS, Robakis NK. An Alternative Secretase Cleavage Produces Soluble Alzheimer Amyloid Precursor Protein Containing a Potentially Amyloidogenic Sequence. *J Neurochem*. 1992;59(6):2328-2331. doi:https://doi.org/10.1111/j.1471-4159.1992.tb10128.x

5. Kinney JW, Bemiller SM, Murtishaw AS, Leisgang AM, Salazar AM, Lamb BT. Inflammation as a central mechanism in Alzheimer's disease. *Alzheimers Dement Transl Res Clin Interv*. 2018;4(1):575-590. doi:https://doi.org/10.1016/j.trci.2018.06.014

6. Role of Tau Protein in Both Physiological and Pathological Conditions | Physiological Reviews. Accessed April 3, 2021. https://journals.physiology.org/doi/full/10.1152/physrev.00024.2003

7. Alonso A del C, Grundke-Iqbal I, Barra HS, Iqbal K. Abnormal phosphorylation of tau and the mechanism of Alzheimer neurofibrillary degeneration: Sequestration of microtubule-associated proteins 1 and 2 and the disassembly of microtubules by the abnormal tau. *Proc Natl Acad Sci*. 1997;94(1):298-303. doi:10.1073/pnas.94.1.298

8. Hyperphosphorylation of Microtubule-Associated Protein Tau: A Pro...: Ingenta Connect. Accessed April 3, 2021. https://www.ingentaconnect.com/content/ben/cmc/2008/00000015/00000023/art00002

9. Jack CR, Albert M, Knopman DS, et al. Introduction to Revised Criteria for the Diagnosis of Alzheimer's Disease: National Institute on Aging and the Alzheimer Association Workgroups. *Alzheimers Dement J Alzheimers Assoc*. 2011;7(3):257-262. doi:10.1016/j.jalz.2011.03.004

10. Du H, Guo L, Fang F, et al. Cyclophilin D deficiency attenuates mitochondrial and neuronal perturbation and ameliorates learning and memory in Alzheimer's disease. *Nat Med*. 2008;14(10):1097-1105. doi:10.1038/nm.1868

11. Cheignon C, Tomas M, Bonnefont-Rousselot D, Faller P, Hureau C, Collin F. Oxidative stress and the amyloid beta peptide in Alzheimer's disease. *Redox Biol*. 2018;14:450-464. doi:10.1016/j.redox.2017.10.014

12. Schinzel AC, Takeuchi O, Huang Z, et al. Cyclophilin D is a component of mitochondrial permeability transition and mediates neuronal cell death after focal cerebral ischemia. *Proc Natl Acad Sci*. 2005;102(34):12005-12010. doi:10.1073/pnas.0505294102

13. Nigro P, Pompilio G, Capogrossi MC. Cyclophilin A: a key player for human disease. *Cell Death Dis*. 2013;4(10):e888-e888. doi:10.1038/cddis.2013.410

14. Melo A, Monteiro L, Lima RMF, de Oliveira DM, de Cerqueira MD, El-Bachá RS. Oxidative Stress in Neurodegenerative Diseases: Mechanisms and Therapeutic Perspectives. *Oxid Med Cell Longev*. 2011;2011:e467180. doi:10.1155/2011/467180

15. Jin Zheng-Gen, Melaragno Matthew G., Liao Duan-Fang, et al. Cyclophilin A Is a Secreted Growth Factor Induced by Oxidative Stress. *Circ Res*. 2000;87(9):789-796. doi:10.1161/01.RES.87.9.789

16. Bell RD, Winkler EA, Singh I, et al. Apolipoprotein E controls cerebrovascular integrity via cyclophilin A. *Nature*. 2012;485(7399):512-516. doi:10.1038/nature11087

17. Kanyenda LJ, Verdile G, Boulos S, et al. The Dynamics of CD147 in Alzheimer's Disease Development and Pathology. *J Alzheimers Dis*. 2011;26(4):593-605. doi:10.3233/JAD-2011-110584

18. Spisni E, Valerii MC, Manerba M, et al. Effect of copper on extracellular levels of key pro-inflammatory molecules in hypothalamic GN11 and primary neurons. *NeuroToxicology*. 2009;30(4):605-612. doi:10.1016/j.neuro.2009.03.005

19. Handschumacher RE, Harding MW, Rice J, Drugge RJ, Speicher DW. Cyclophilin: a specific cytosolic binding protein for cyclosporin A. *Science*. 1984;226(4674):544-547. doi:10.1126/science.6238408

20. Emmel EA, Verweij CL, Durand DB, Higgins KM, Lacy E, Crabtree GR. Cyclosporin A specifically inhibits function of nuclear proteins involved in T cell activation. *Science*. 1989;246(4937):1617-1620. doi:10.1126/science.2595372

21. Borel JF, Feurer C, Magnée C, Stähelin H. Effects of the new anti-lymphocytic peptide cyclosporin A in animals. *Immunology*. 1977;32(6):1017-1025.

22. Stähelin HF. The history of cyclosporin A (Sandimmune®) revisited: Another point of view. *Experientia*. 1996;52(1):5-13. doi:10.1007/BF01922409

23. Flisiak R, Feinman SV, Jablkowski M, et al. The cyclophilin inhibitor Debio 025 combined with PEG IFNα2a significantly reduces viral load in treatment-naïve hepatitis C patients. *Hepatology*. 2009;49(5):1460-1468. doi:https://doi.org/10.1002/hep.22835